ARTICLES

Single Molecule Rotational and Translational Diffusion Observed by Near-Field Scanning Optical Microscopy

A. G. T. Ruiter,*,† J. A. Veerman, M. F. Garcia-Parajo, and N. F. van Hulst

Applied Optics Group and MESA Research Institute, Department of Applied Physics, University of Twente, P.O. Box 217, 7500 AE Enschede, The Netherlands

Received: March 25, 1997; In Final Form: June 23, 1997[⊗]

We have observed rotational and translational diffusion of single molecules using a near-field scanning optical microscope with two polarization detection channels. The measurements were performed under ambient conditions with the molecules dispersed on glass or embedded in polymer. In successive images the fluorescence of single molecules was followed over about 1 h, with 10 ms integration time, until photodissociation. The position of single molecular fluorescence could be located with an accuracy of 1 nm. From the lateral diffusion of Rhodamine 6G molecules on glass during successive images, a diffusion constant of $(6.7 \pm 4.5) \times 10^{-15}$ cm^2/s was determined. The orientation of the in-plane emission dipole of all molecules in one image could be directly determined with an accuracy of a few degrees by simultaneous detection in two perpendicular polarization directions. By rotating the excitation polarization we could selectively excite different sets of molecules and compare their in-plane absorption and emission dipole orientation. Monitoring DiI molecules in PMMA over 1 h, we found rotation of less than 10° for the majority of molecules, while incidental fast rotation and transition to a dark state occurs. The fluorescence intensity was observed to be molecule dependent, which is an indication for out-of-plane orientation and different local photophysical environment.

Introduction

Recent advances in single-molecule detection and spectroscopy have opened the possibility to investigate the physical and chemical environment at the molecular level. In earlier experiments, laser-cooled ions were confined in an electromagnetic trap in vacuum,[1,2] giving a high spectral resolution of the isolated ion. Later experiments reported on the spectral selection of single impurities in a solid matrix[3,4] by tuning the excitation wavelength to the absorption band of a single molecule. Information on the specific local environment of the selected molecule could thus be extracted. During the last decade, improvement in the efficiency of photodetectors[5] and the introduction of scanning (probe) microscopes have taken the single-molecule studies out of the vacuum chamber and created the possibility to observe single molecules at ambient conditions. The first true imaging of immobilized single dye molecules by optical means at room temperature was achieved by near-field scanning optical microscopy (NSOM).[6] Several exciting single-molecule experiments have been performed since then. The emission spectrum of a single molecule at various conditions was detected using both near-field[7] and far-field methods,[8−10] revealing single-molecule spectral jumps. Single-molecular fluorescence lifetimes were determined[8] showing the local photophysical heterogeneity[11] and the influence of nonradiative quenching in the presence of an aluminum-coated probe.[12−14] All these advances show that single-molecule experiments indeed provide a sensitive tool to study the local environment of a single molecule at ambient conditions.[15]

For many applications, it is of major importance to follow dynamic processes like diffusive motion and redistribution of components in polymers and biological membranes. Translational (lateral) diffusion is directly important because it often determines the kinetic rate of certain chemical reactions. Recently, imaging of single-molecule lateral diffusion has been achieved using sensitive fluorescence microscopy either in the far-field,[16,17] with a time resolution into the millisecond range, or in the near-field,[18] where the trajectory of the molecule could be recorded during more than 1 h at the expense of lower time resolution. Single-molecule rotational diffusion, recently observed using far-field,[19] is likewise interesting because it is more sensitive to molecular size and shape than translational diffusion. The exact determination of the molecular orientation is of vital importance in fluorescence resonance energy transfer experiments[20] and in the study of time-dependent phenomena such as protein and molecular conformational changes.

We have optimized our near-field optical microscope[21,22] for fluorescence imaging of single molecules with efficient optical signal detection and background rejection, combined with long-term stability and high spatial resolution. In the detection path, the fluorescence signal was separated in two perpendicular polarization directions and detected with two photon-counting avalanche photodiodes. By monitoring the relative contributions of both polarization components, the in-plane orientation of all molecular dipoles in one image could be directly determined. Thus, rotational diffusion and reorientation of single molecules on the $10^{-2}-10^{3}$ s time scale was readily visualized and analyzed.

Experimental Section

The experimental setup is schematically shown in Figure 1. The NSOM was built into a Zeiss Axiovert 135 TV inverted

† E-mail: A.G.T.Ruiter@tn.utwente.nl.

⊗ Abstract published in *Advance ACS Abstracts,* September 1, 1997.

S1089-5639(97)01066-9 CCC: $14.00

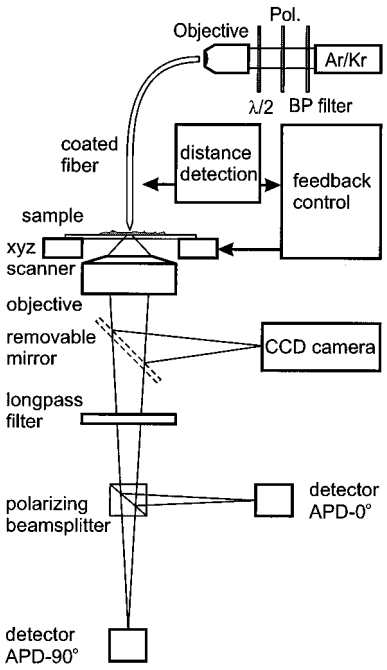

Figure 1. Near-field scanning optical microscope configuration. The tip−sample distance is controlled using tuning fork shear-force feedback. Both detectors are photon-counting avalanche photodiodes.

optical microscope.[23] A subwavelength light source was used to illuminate the sample. The light source consisted of a tapered, aluminum-coated single mode optical fiber (Newport F-SV) with an aperture of approximately 100 nm. The 514 nm line from an Ar/Kr laser was used as the excitation wavelength and coupled into the coated fiber. The sample was scanned underneath the fiber and the fluorescence emission from the sample plane was collected with a 100×, 1.3 NA oil immersion objective and directed to the detectors. The fluorescence was filtered from the transmitted light using a longpass filter (550 nm). A broadband polarizing beamsplitter cube (Newport, 400−700 nm) was used to separate the fluorescence signal into two perpendicular polarization components which were then sent to the detection channels. Photon-counting avalanche photodiodes (APD, SPCM-100 from EG&G Electro Optics) were used as detectors, which were confocally aligned with the fiber aperture. Shear force feedback based on a tuning fork system[24,25] was used to maintain a constant tip−sample separation, using a dither amplitude less than 1 nm. The tip−sample distance was typically a few nanometers with a noise level of approximately 1 nm. A personal computer controlled the raster scanning of the sample, collected the counts per pixel for each detector, and digitized the z-piezo voltage to create a height image of the sample. For excitation polarization experiments, a polarizer and a rotatable $\lambda/2$ plate were placed in the optical path before the coupling of the light into the fiber. The extinction ratio usually was better than five in the two perpendicular polarization directions.

Background fluorescence from the fiber tip itself was minimized by keeping its length as short as possible (less than 15 cm length) and removing its plastic jacket. The detection efficiency of the optical path was optimized for maximum signal collection (collection efficiency was approximately 10%, including quantum efficiency of the APD detectors). With an excitation power of typically 3 nW at the end of the coated tip (as measured in the far field) count rates between 10^3 and 10^4 counts/s per detector from a single molecule were obtained at a background signal of typically 300 counts/s per detector. By imaging a sample area of a few square microns approximately

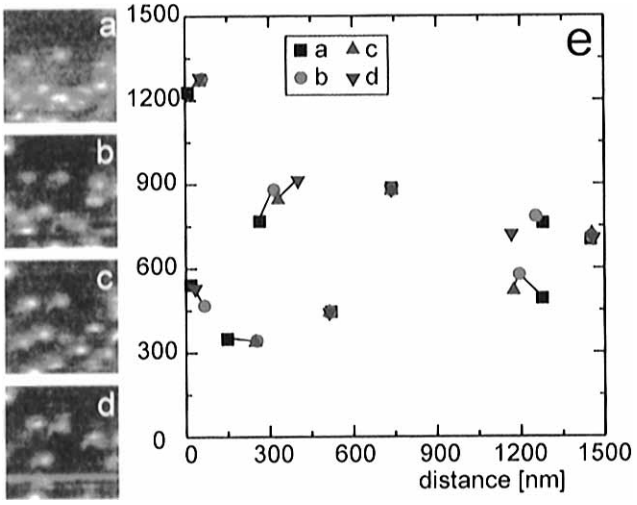

Figure 2. Four consecutive single molecule images (a−d) of R-6G molecules on glass. The images are 1.5 × 1.5 μm at 100 × 100 pixels. The measurement time is 10 min per image. (e) Shows the relative movement of the molecules in the images, after compensation for the average drift.

once every 10 min, the molecules in this area could be traced over more than an hour.

Rhodamine 6G (R-6G) and carbocyanine (DiI-C_{18}) dye molecules were chosen because of their high photostability, well-known photophysical properties, and relevance as cell-membrane and/or oligonucleotide probes. Some samples were prepared by directly spin coating a 5×10^{-8} M solution of the dye molecules in methanol on a clean 170 μm thick glass cover glass. A second set of samples was prepared by spin coating the dye solution on a thin poly(methyl methacrylate) (PMMA) layer. The polymer layer was prepared by spinning a solution of 0.5 wt % PMMA in chloroform on a clean glass coverslip at 4000 rpm resulting in a layer thickness between 5 and 10 nm. A third set of samples was prepared by spin coating a solution of PMMA, already containing the molecules, onto a clean glass coverslip, in order to have the molecules embedded in the polymer layer. In all three types of samples the resulting coverage was typically a few dye molecules per square micrometer.

Results and Discussion

Lateral Diffusion. Figure 2(a−d) shows four consecutive images of individual R-6G molecules adsorbed on a glass substrate. In these measurements a single APD detector was used, without the polarizing beamsplitter. The integration time per pixel was 25 ms, resulting in a background signal of 15 counts/pixel and a maximum signal of ∼100 counts/pixel. The total measurement time per image was 10 min. Figure 2e displays the relative positions of the molecules shown in the four consecutive images over the 1.5 × 1.5 μm (100 × 100 pixels) image region. The positions were calculated by taking their weighted center. After compensation for the instrumentation drift, translational movement of some individual molecules over the glass surface can be readily observed. While some molecules appear to be well located and fixed at the sample surface from frame to frame, some other molecules show translational trajectories over 100 nm in time spans of 10 min. From our data, the center of intensity of the different molecules can be determined[26] with an accuracy of approximately 1 nm.

Several possible mechanisms can contribute to the translation of the center fluorescence intensity location of a single molecule over the sample surface. First, thermally induced diffusion of

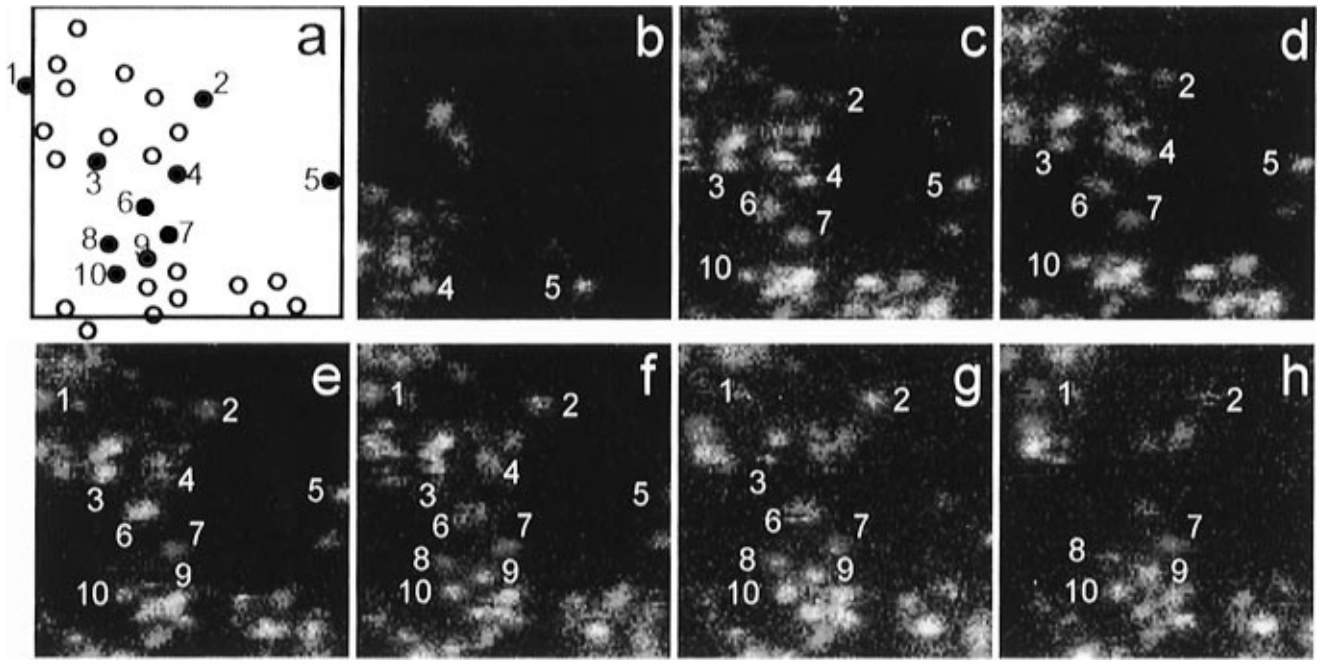

Figure 3. Seven consecutive single molecule images of DiI molecules on PMMA. A color coding has been introduced to illustrate the relative contributions of the two perpendicular polarized fluorescence intensities (see text for details). Each image has a scan range of 1.5 × 1.5 μm and the measurement time per image was 10 min. (a) Shows the relative positions of the molecules with some individual molecules depicted with a number.

the molecules over the glass−air surface can occur. Recently, this process has been observed at R-6G molecules embedded in a solid polymer host using a near-field optical microscope[18] reporting a diffusion constant of $(2.6 \pm 0.2) \times 10^{-15}$ cm^2/s for that system. From Figure 2e, a diffusion constant can be derived by calculating the mean square displacement, MSD, as a function of time lags (τ) between the images:

$$\mathrm{MSD}(\tau) = \frac{1}{\sum_{\tau = t_i - t_j} 1} \sum_{\tau = t_i - t_j} (\vec{r}(t_i) - \vec{r}(t_j))^2$$

where $\vec{r}(t)$ represents the position of the molecule at time t. The lateral diffusion constant, D, for two dimensional diffusion is given by $\mathrm{MSD}(\tau) = 4\,D\tau$. Using this equation, a diffusion constant of $(6.7 \pm 4.5) \times 10^{-15}$ cm^2/s is calculated, averaging over molecules in Figure 2e.

Second, apparent lateral diffusion may be observed, being in fact the result of differences on the spatial location of the maximum of the fluorescence intensity while no translation of the molecule occurs. The field from the aperture illuminating the molecule is nonhomogeneous in strength and in polarization direction.[27,28] As a consequence, the location of maximum overlap between the absorption dipole of the molecule and the emerging field from the tip will depend on the orientation of the dipole. On rotation of the molecule, a shift in the maximum fluorescence intensity location may occur which can extend up to the aperture size.[18] Rotational diffusion of the molecules occurs at a shorter time scale than lateral diffusion, giving rise to a nonlinear behavior of the MSD(τ) when evaluated at the molecular rotation time scale. At the time scale of lateral diffusion this can be regarded as an offset at time $\tau = 0$, MSD-(τ) $= M_0 + 4\,D\tau$, so the slope of the MSD still reveals the correct lateral diffusion constant. Identically, intensity fluctuations on the time scale of a few line scans, which could be due to spectral jumps or going to a dark state, would result in an offset of the MSD and yield the same slope and diffusion constant.

Finally, the observed lateral mobility can be induced by interactions between fiber and molecule. Indeed, occasionally we have observed the attachment of a molecule to the probe, resulting in a continuous fluorescence signal during a time period up to a second, eventually ending in photodissociation or detachment. The location where the molecule detached from the probe could be clearly identified in the subsequent scanline. The presence of a thin water contamination layer on top of the sample surface can increase the probability of a probe-induced process, because the probe is believed to drag through this layer while scanning over the sample surface, as extensively studied with atomic force microscopy.[29,30] However, in these rare cases the lateral diffusion would have a preferential direction along the horizontal scan direction. Therefore, the random direction of molecular mobility, as observed in Figure 2, makes the occurrence of direct tip-induced effects improbable. However, tip heating can increase the diffusion rate at the molecules close to the tip, although this effect can only give rise to temporal temperature increases of a few tens of degrees, during a few percent of the total measurement time. Laser desorption due to transient heating could cause an increase in diffusion rate. To rule out these probe-induced effects, measurements could be performed with different integration times, or a different delay time between successive scans.

Rotational Diffusion. Figure 3 shows seven consecutive images of individual DiI molecules on a PMMA layer, where image (b) has been intentionally displaced with respect to images (c) to (h). The image scan range was 1.5 × 1.5 μm, taking 100 × 100 pixels with an integration time of 25 ms per pixel. Measuring on both forward and backward scan resulted in a measurement time of 10 min per image. Each image consists of two data sets, one for each detector. We have colored the data from the 0°-detector red and the data from the 90° detector, detecting the perpendicularly polarized fluorescence, green. Finally, both data have been added up to create one image. Therefore, each image should be viewed as the addition of two data sets, one per detector, reflecting the relative contributions of each polarization component, where equal amounts of red

and green give yellow. In what follows, the two polarization directions will be referred to as the "red" and "green" direction. The peak intensity was about 90 counts/pixel per detector and the background signal was about 10 counts/pixel per detector. The images display raw data without any smoothing of filtering; only the background count rate was subtracted and the maximum was clipped at 55 counts.

Several interesting features can be observed by following the behavior of some of the molecules from image to image. Molecule 7 remains fixed with a stationary dipole along the "green" direction from images (c) to (h), on a time scale of 1 h without photodissociation. Stationary dipoles are also observed for molecule 3 until sudden bleaching occurs during the scanning of image (g), for molecule 10 from images (c) to (h) and for molecule 5 from images (b) to (e). These features and their reproducibility from frame to frame demonstrate the stability of our set-up and the reliability of our detection system. In particular, molecules 4 and 5 in images (b)−(d) do have different intensity contributions: while the intensity of molecule 5 remains essentially constant from frame to frame, the relative intensity of molecule 4 changes from frame to frame, thus excluding changes in the excitation.

While some molecules show stationary dipoles on a 10^3 s time scale, and some other molecules show rotational activity from frame to frame or even within one image. This is the case for molecule 4 as mentioned above, which appears to gradually rotate from the "red" direction toward the "green" between images (b) to (d) and back again to "red" direction from images (f) to (h). Fast rotational activity is observed for molecule 6 with sudden fluctuations from one scan line to the other within the same image.

Sudden appearance of molecules is also observed on the time scale of our measurements. For instance, molecules 8 and 9 are clearly present only after image (f). The same occurs with molecule 2 which is present only after image (d) showing also certain rotational activity. An on−off−on behavior is observed by molecule 1 which emits light in frames (e), (f), and (h) but it is absent during image (g). The sudden appearance/disappearance of molecules can be attributed to rotation or to sudden changes in the molecular photophysics. The first argument requires a sudden rotation of the molecular dipole perpendicular to the excitation polarization and subsequent reorientation to the original in-plane orientation to start reemitting fluorescence, which is unlikely. We believe in the second argument, where the molecule retains its orientation, while making a temporary transition to a dark nonemitting state[19] or a spectral jump[8,10,12] away from the laser wavelength.

Determination of the Molecular Orientation. Using linearly polarized light, molecules with their absorption dipole oriented parallel to the excitation polarization are selectively excited whereas molecules with their absorption dipole perpendicular to the excitation are not. Figure 4 shows a series of four consecutive images of DiI molecules in a thin PMMA layer over the same area. The image size is 3 × 3 μm (200 × 200 pixels), with a pixel integration time of 10 ms adding up to about 15 min per image. The polarization directions of the two detection channels were colored red (0°) and green (90°). The excitation polarization direction was rotated from 90° via 0° and 45° to −45° for images (a)−(d), respectively.

It can be observed that each image reveals a different distribution of molecules. Some molecules which are present in the one image are absent in the other, and vice versa. Image (a) shows mainly green-colored molecules, as the excitation was parallel to the "green" detection channel. Image (b) shows mainly red molecules, for the excitation was rotated 90° to the

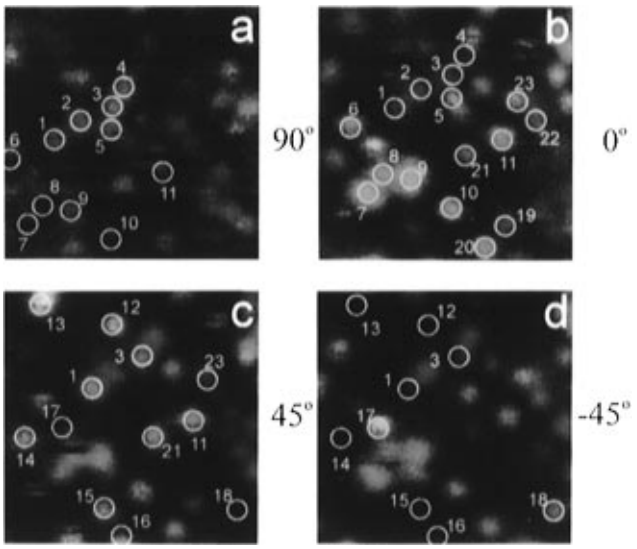

Figure 4. Four consecutive single molecule images of DiI molecules in a 10 nm thick PMMA layer. The scan area is 3 × 3μm at 200 × 200 pixels with an integration time of 10 ms per pixel. The excitation polarization was oriented (a) 90°, (b) 0°, (c) 45°, and (d) −45°.

"red" detection channel. From this observation it can be concluded that the absorption and emission dipole of the molecule are oriented approximately parallel. The color of most of the molecules remained constant during imaging, indicating a fixed orientation.

By comparing images (a) and (b), one can see that the green-colored molecules 1−4 in image (a) are hardly visible in image (b), so they are oriented mainly in the 90° direction. Molecule 5 changes from green in image (a) to red in image (b), and has disappeared in subsequent images, which could be a rotation followed by bleaching. The red molecules 6−11 of image (b) are not visible in image (a), so they must be oriented mainly in the 0° direction. A similar comparison can be made between images (c) and (d), which correspond to the 45° and −45° excitation, respectively. For example, molecules 1, 3, and 12−16 are only visible in image (c), while molecules 17 and 18 are only visible in image (d).

Similarly to Figure 3 also Figure 4 shows molecules disappearing and reappearing within the same image. For example, molecule 8 in Figure 4c vanishes during a few scan lines after which it reappears (Figure 4d) in its original orientation; see Table 1. A similar behavior in image (c) is observed at the molecule left of molecule 16. This molecule displays transitions between emitting and nonemitting state and vice versa over a few pixels (10−100 ms) and over several scan lines (1−10 s). Because the orientation of the molecules prior to disappearance and after reappearance is identical, a rotational effect of the molecule can be excluded. The observations can be attributed to a temporary transition to a dark state or a spectral jump.

For every observable molecule the angle between the "red" detection direction (0°) and the in-plane component of the emission dipole of the molecule can be derived in a single measurement. This is done by calculating the arc-tangent of the square root of the ratio of the measured integrated intensities of the molecule in the two detection channels, taking into account the background counts in each channel. Still, in doing so no information on the sign of the angle is obtained. However, assuming that the angle between the molecular absorption and emission dipole is zero, which is a good approximation in the case of DiI,[31,32] the absolute angle can be determined by rotating the excitation polarization and comparing the relative intensities between the various measurements. The calculated absolute

TABLE 1: In-Plane Molecular Emission Dipole Angles in Degrees for All 23 Molecules Displayed in Figure 4, for All Four Excitation Polarizations

no.	90° Figure 4a	0° Figure 4b	45° Figure 4c	−45° Figure 4d
1	68 ± 2	59 ± 3	56.8 ± 0.7	
2	69 ± 1	59 ± 3	63 ± 1	68 ± 2
3	65 ± 1	57 ± 3	60.8 ± 0.8	64 ± 3
4	71 ± 1	60 ± 5	71 ± 1	68 ± 2
5	72 ± 2	26 ± 1		
6	8 ± 17	12 ± 2	7 ± 6	
7	−19 ± 12	−18 ± 1	−18 ± 2	−16 ± 1
8		−14 ± 2		−16 ± 2
9		20 ± 1	26 ± 1	19 ± 1
10		9 ± 2	9 ± 3	7 ± 4
11	22 ± 7	14 ± 2	13 ± 2	10 ± 4
12	49 ± 2	40 ± 2	36.6 ± 0.7	
13	55 ± 1	50 ± 2	46.7 ± 0.6	
14		25 ± 2	44 ± 1	
15	45 ± 2	41 ± 2	37.1 ± 0.9	
16		40 ± 3	37 ± 1	
17		−32 ± 1	−28 ± 3	−35.5 ± 0.7
18		−48 ± 2		−36 ± 1
19	69 ± 3	62 ± 3	63 ± 2	
20		13 ± 2	16 ± 2	15 ± 2
21	39 ± 2	28 ± 2	27 ± 1	28 ± 4
22	−60 ± 2	−48 ± 2	−46 ± 3	−54 ± 1
23	−61 ± 2	−39 ± 1	−58 ± 2	−43 ± 1

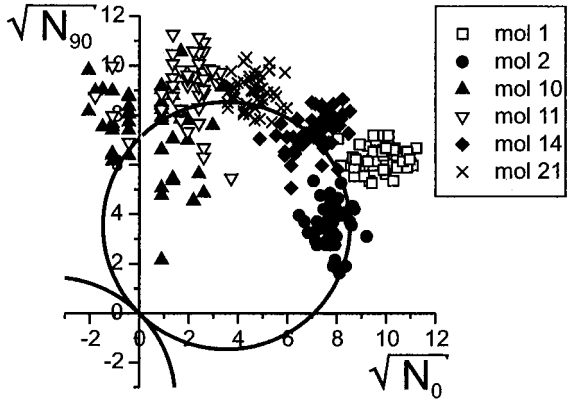

Figure 5. Scatter plot of the square root of the counts per pixel in the 90° detector ($\sqrt{N_{90}}$) vs the square root of the counts per pixel in the 0° detector ($\sqrt{N_0}$), for 6 molecules from Figure 4c with 49 pixels per molecule. The solid line represents the theoretical detection response for molecules excited with light polarized with an angle of 45°.

angles for the numbered molecules in each of the four images of Figure 4 are listed in Table 1. From this table it is noticed that for molecules oriented along the excitation polarization the angle of the emission dipole of a molecule could be determined with an error of only a few degrees. The error increases for molecules oriented far from the excitation polarization due to the decreased signal to noise ratio. In order to verify the values found in Table 1, an identical calculation was performed on data measured on the backward scan direction (not shown here). The angles calculated from that data set were in agreement with Table 1.

In order to simultaneously quantify the molecular orientation and the fluorescence intensity of a single molecule, a scatter plot of the square root of the counts per pixel in the 90° detector vs the square root of the counts per pixel in the 0° detector was made. In Figure 5 this was done for six molecules taken from Figure 4c. For each molecule the counts of 49 pixels (in an area with a radius of 4 pixels around the molecule) are displayed. For each pixel the average background per detector was subtracted. With an excitation polarization at 45° and for molecules with an in-plane angle φ the relative intensities measured at the two detectors are $I_0 \sim \cos^2(\varphi - 45)\cos^2(\varphi)$ and $I_{90} \sim \cos^2(\varphi - 45)\sin^2(\varphi)$, assuming the emission and absorption dipole parallel. The solid line in Figure 5 displays the theoretical detection response curve for in-plane molecules excited under 45° where the absolute scale of the curve was fitted to the data. The good correspondence between the data and the theoretical curve confirms that absorption and emission dipole of the DiI molecules are oriented approximately parallel. It is interesting to notice that in Figure 5 molecules 1 and 2 display a different intensity, despite their almost parallel orientation. This can be explained by two effects.

First, and most likely, molecule 2 is rotated out of plane, decreasing the overlap with the excitation and lowering the detection efficiency. Betzig *et al.*[6] reported the observation of field profiles at the aperture according to the theory derived by Bethe[27] and Bouwkamp.[28] Figures 3 and 4 do not confirm the presence of these characteristic field components. This is most likely due to the imperfect quality of the probe, which does not satisfy the model of a perfect aperture, i.e., flat circular end face surrounded by a homogeneous metal film.

Second, inhomogeneity of the local environment of the molecules and their different proximity to the aluminum probe affects the radiative decay rate,[10−14] resulting in intensity differences from molecule to molecule.

Conclusions

Fluorescence from single molecules could be localized with a resolution of approximately 1 nm, due to the subdiffraction-limited resolution of the near-field scanning optical microscope. The trajectories of R6G molecules on glass have been monitored over an hour. The molecular mobility is attributed to thermal diffusion. A probe-induced process could also influence the diffusion; however, no preferential movement along the scan direction was observed. A lateral diffusion constant of $(6.7 \pm 4.5) \times 10^{-15}$ cm^2/s was determined.

The benefits of a polarization discriminating detection scheme in a near-field optical microscope have been demonstrated. Molecular dipole orientations could readily be determined for all molecule in a single image, showing the possibility of investigating single molecule rotational diffusion on a time scale of 10^{-2}−10^3 s, while simultaneously locating the molecular fluorescence with an accuracy of about 1 nm. DiI molecules on and in a PMMA layer were shown to rotate on a time scale of minutes, indicating a much lower translational diffusion constant as compared to the diffusion constant found for R6G molecules on glass. Using different excitation polarizations the absolute dipole orientation of stationary single molecules has been determined. The angle of the in-plane dipole orientation was measured with an accuracy of a few degrees. The absorption and emission dipole orientations of DiI molecules were measured to be approximately parallel.

Acknowledgment. We acknowledge Marco Moers, Kees van der Werf, and Frans Segerink for their technical support and advise in the design of the near-field optical microscope. T.R. and J.-A.V. gratefully acknowledge the Dutch Organization for Fundamental Research on Matter (FOM) for their financial support. M.F.G.-P. is supported by the European HCM network on "Near-field optics for nano-scale science and technology".

References and Notes

(1) Itano, W. M.; Bergquist, J. C.; Wineland, D. J. *Science* **1987**, *237*, 612.
(2) Diedrich, F.; Walther, H. *Phys. Rev. Lett.* **1987**, *58*, 203.
(3) Moerner, W. E.; Kador, L. *Phys. Rev. Lett.* **1989**, *62*, 2535.
(4) Orrit, M.; Bernard, J. *Phys. Rev. Lett.* **1990**, *65*, 2716.
(5) Li, L-Q.; Davis, L. M. *Rev. Sci. Instrum.* **1993**, *64* (6), 1524.

(6) Betzig, E.; Chichester, R. J. *Science* **1993**, *262*, 1422.
(7) Trautman, J. K.; Macklin, J. J.; Brus, L. E.; Betzig, E. *Nature* **1994**, *369*, 40.
(8) Trautman, J. K.; Macklin, J. J. *Chem. Phys.* **1996**, *205*, 221.
(9) Lu, H. P.; Xie, X. S. *Nature* **1997**, *385*, 143.
(10) Xie, X. S. *Acc. Chem. Res.* **1996**, *29*, 598.
(11) Macklin, J. J.; Trautman, J. K.; Harris, T. D.; Brus, L. E. *Science* **1996**, *272*, 255.
(12) Xie, X.; Dunn, R. C. *Science* **1994**, *265*, 361.
(13) Ambrose, W. P.; Goodwin, P. M.; Martin, J. C.; Keller, R. A. *Science* **1994**, *265*, 364.
(14) Bian, R. X.; Dunn, R. C.; Xie, X. S. *Phys. Rev. Lett.* **1995**, *75*, 4772.
(15) Dunn, R. C.; Holtom, G. R.; Mets, L.; Xie, X. S. *J. Phys. Chem.* **1994**, *98*, 3094.
(16) Schmidt, Th.; Schütz, G. J.; Baumgartner, W.; Gruber, H. J.; Schindler, H. *Proc. Natl. Acad. Sci. U.S.A. Biophysics* **1996**, *93*, 2926.
(17) Schmidt, Th.; Schütz, G. J.; Baumgartner, W.; Gruber, H. J.; Schindler, H. *J. Phys. Chem.* **1995**, *99*, 17662.
(18) Bopp, M. A.; Meixner, A. J.; Tarrach, G.; Zschokke-Graenacher, I.; Novotny, L. *Chem. Phys. Lett.* **1996**, *263*, 721.
(19) Ha, T.; Enderle, Th.; Chemla, D. S.; Selvin, P. R.; Weiss, S. *Phys. Rev. Lett.* **1996**, *77*, 3979.
(20) Ha, T.; Enderle, Th.; Ogletree, D. F.; Chemla, D. S.; Selvin, P. R.; Weiss, S. *Proc. Natl. Acad. Sci. U.S.A.* **1996**, 93, 624.
(21) Moers, M. H. P.; Gaub, H. E.; van Hulst, N. F. *Langmuir* **1994**, *10*, 2774.
(22) Moers, M. H. P.; Kalle, W. H. J.; Ruiter, A. G. T.; Wiegant, J. C. A. G.; Raap, A. K.; Greve, J.; De Grooth, B. G.; van Hulst, N. F. *J. Microsc.* **1996**, *182*, 40.
(23) van Hulst, N. F.; Moers, M. H. P. *IEEE—Eng. Med. Biol.* **1996**, 51.
(24) Karrai, K.; Grober, R. D. *Appl. Phys. Lett.* **1995**, *66* (14), 1842.
(25) Ruiter, A. G. T.; Veerman, J. A.; v/d Werf, K. O.; van Hulst, N. F. *Appl. Phys. Lett.* **1997**, *71* (1), 28.
(26) Bobroff, N. *Rev. Sci. Instrum.* **1986**, *57*, 1152.
(27) Bethe, H. A. *Phys. Rev.* **1944**, *66*, 163.
(28) Bouwkamp, C. J. *Philips Res. Rep.* **1950**, *5*, 401.
(29) Weisenhorn, A. L.; Hansma, P. K.; Albrecht, T. E.; Quate, C. F. *Appl. Phys. Lett.* **1989**, *54*, 2651.
(30) Salmeron, M.; Neubauer, G.; Folch, A.; Tomitori, M.; Ogletree, D. F.; Sautet, P. *Langmuir* **1993**, *9*, 3600.
(31) Axelrod, D. *Biophys. J.* **1979**, 26, 557.
(32) Velez, M.; Axelrod, D. *Biophys. J.* **1988**, *53*, 575.